Available online at www.sciencedirect.com
ScienceDirect
Polymer 47 (2006) 7289–7301
polymer
www.elsevier.com/locate/polymer

Monte Carlo simulation of linear polymer melts in shear flow. Effect of shear stress and confined space on chain dynamics

Jeremiasz K. Jeszka [a,b,*], Tadeusz Pakula [a,c]

[a] Department of Molecular Physics, Technical University of Lodz, 90-924 Lodz, Poland
[b] Centre for Molecular and Macromolecular Studies, Polish Academy of Sciences, 90-363 Lodz, Poland
[c] Max-Planck Institute for Polymer Research, D-55021 Mainz, Germany

Received 19 January 2006; received in revised form 21 March 2006; accepted 5 April 2006
Available online 30 June 2006

Abstract

Linear homopolymer melts under shear stress were studied using a Monte Carlo method in a dense system, using the cooperative motion algorithm. The simulations were performed in a plane-parallel geometry, between reflective walls, for chains up to 640 beads (entangled). Behavior of the melts under shear stress was simulated by appropriate biasing of the bead move probability. Chain dynamics was monitored during reaching the equilibrium flow in the step-shear experiment (creep) simulation, in the equilibrium flow and during melt relaxation. The results were compared with those obtained for non-flowing melt. Significant differences between step-shear and steady-state simulations were observed, while chain dynamics during recovery is almost identical with that in non-flowing melt. Dynamics of the melt depended strongly on the chain length and shear stress, showing nonlinear effects for long chains. Chain orientation, coil deformation and relaxation were analyzed. Relaxation time of long chain decreased by orders of magnitude under shear following the power law. Diffusion of beads and chains was analyzed and an anomalous diffusion was observed, also in the directions perpendicular to the flow direction. In the flowing melt the effect of confined space was important, even if the wall spacing was much bigger than $\boldsymbol{R}_g$.

Keywords: MC simulations; Shear flow; Anomalous diffusion

1. Introduction

Rheological behavior of polymers under shear stress is of great interest both from technological and scientific point of view [1–4]. Practical aspects involve polymer processing and lubrication, also in biological systems. In spite of a large body of results, coming mainly from experiments, the understanding of behavior of polymer melts under shear flow and possibilities of a theoretical description are still limited, especially on the molecular level. Comparing with the relatively well-understood flow of low molecular weight liquids, in polymer melts and solutions we deal with significant changes of chain conformation in the flow field and for long chains also with entanglements. The former effect is well-known and it is believed to be responsible for shear thinning of polymer liquids. Generally polymers show a strong dependence of viscosity on the shear rate (usually described in the first approximation by the well-known power law [1,2]). Providing an insight into the flow induced phenomena on the molecular level such as coil deformation and chain orientation is of great importance. Therefore computer simulations can be very helpful.

The most suitable simulation method is nonequilibrium molecular dynamics (NEMD) applied successfully for simple liquids. A serious drawback of using NEMD for polymers is that the calculations are complex and time consuming, thus the simulations cover relatively short time (up to *ca.* 100 ns) while relaxation times of chains of hundreds of beads are *ca.* 10^5 times longer than those of a single bead. The systems comprising *ca.* 10^4 monomers at most (for simplified models) are used which is

* Corresponding author. Department of Molecular Physics, Technical University of Lodz, 90-924 Lodz, Poland. Tel.: +48 42 6803 228; fax: +48 42 6803 260.
E-mail address: jkjeszka@cbmm.lodz.pl (J.K. Jeszka).

0032-3861/$ - see front matter © 2006 Elsevier Ltd. All rights reserved.
doi:10.1016/j.polymer.2006.04.071

not sufficient to have good averaging of long chain parameters. The results obtained for simple and complex fluids (including polymers) using mostly the finitely extendable nonlinear elastic (FENE) model have been recently summarized in Ref. [5]. It has been found that even simple liquids show shear rate dependent viscosity. The well-known crossover in the zero-shear viscosity, related to entanglements was also obtained. Simulations using detailed models of linear and branched alkanes having up to 30 carbon atoms [6–8] have already shown that such relatively short, not entangled molecules change their conformations and orientation under shear, especially in confined space and in the vicinity of an impenetrable wall.

In Monte Carlo simulations the motions of polymer chains in the melt are considered as a series of random displacements of segments. In the flowing melt such segmental motions are no longer random, but they have a preferred direction resulting from an external stress. This effect can be simulated by modifying probabilities of individual jumps accordingly [9–12]. Several groups used various simulation methods to study macromolecules in solution, there are, however, only few papers reporting simulations of polymer melts under shear flow. Baschnagel and Binder [10] considered the effect of shear deformation of a dense polymer confined between repulsive walls using a coarse-grained bond-fluctuation model. Their system comprised 40^3 beads and typical chain length was 10. Pakula [11] simulated the effect of shear flow on microphase separation of diblock copolymers using the cooperative motion algorithm (chain length 40). Gleiman and Dorgan [12] used the same algorithm to simulate Poiseuille flow of homopolymer melt (up to 256 segments). In all the cases chain deformation and orientation were found, and in Refs. [10] and [12] also an influence of the walls was observed. Mavrantzas and Theodoru [13,14] performed atomistic Monte Carlo simulations of elongation flow of polyethylene melt in atomistic detail (up to 1000 united atoms) using their end-bridging algorithm. They obtained linear dependence of chain orientation and conformation tensor on the stress difference, conformity to the stress optical law and melt viscosity for shorter, unentangled chains.

Regardless of the method employed, simulations of the dynamics of long polymer chains can be performed in a reasonable time only using the coarse-grained approximations. The effectiveness of the simulation algorithm is crucial for the simulation of melt flow because due to the long range effects the simulated system must be big enough and long relaxation times of big macromolecules need simulation of the long time behavior – at least four orders of magnitude longer than for small molecules. Among various simulation methods used to represent behavior of polymers the cooperative motion algorithm (CMA) [15–18] used in the present work is a unique one because it allows to simulate really dense systems, corresponding to polymer melts and it is sufficiently efficient.

In the present work we study the behavior of homopolymer melts between the repulsive walls under shear stress, simulated using a simple bias field. Jump probability bias is linearly dependent on bead position with respect to impenetrable walls, which reproduces well behavior of simple liquids in Couette flow. In contrast to Poiseuille flow profile used in Ref. [12] it allows a straightforward analysis of the influence of stress and stress gradient on various parameters. However, as we demonstrate, for longer molecules the flow profile of the polymer melt is different and depends nonlinearly on the molecular weight and on the shear stress. We study in detail chain dynamics in four cases corresponding to step-shear (creep), steady-state flow and melt relaxation experiments, in comparison with non-flowing melts of the same chain length between repulsive walls. The effect of the confined space (the distance between the walls) cannot be avoided in such simulations and is also discussed. Broad range of chain length studied makes possible better analysis of shear and confinement effects, also for entangled melts.

2. Simulation method

In the simulations using cooperative motion algorithm (CMA) ensembles of beads located at lattice sites are connected by non-breakable bonds to form structures representing macromolecules of various topologies [15–20]. All the lattice sites are occupied in order to represent dense systems, like polymer melts. The presented results are obtained by simulations on an fcc lattice, where the bonds have length $a = \sqrt{2}$. The possible bond angles are $\alpha = 60°$, $90°$, $120°$ and $180°$ with degeneracy $d_\alpha = 2$, 4, 2 and 1, respectively. The coordination number of the lattice is equal to 12, i.e., every monomer has 12 nearest neighbors.

The systems are considered under the excluded volume condition, which means that each lattice site can only be occupied by a single molecular element (bead). In such systems strictly cooperative dynamics is used, consisting in rearrangements satisfying local continuity of the simulated system (no empty lattice sites are generated). A segment of one chain can move only if other segments of different chains move simultaneously. This is realized by local motions consisting in displacements of a certain number of molecular elements along closed loops, so that each element replaces one of its neighbors in such a way that the sum of displacements of the elements taking part in the rearrangement is zero (continuity condition). During such rearrangements the model macromolecules undergo conformational transformations, preserving, however, their identities given by the number and the sequences of elements in the polymer. Monitoring positions and/or orientations of chain elements in time allows to detect the dynamics in such a system. Quantities characterizing the system are calculated only between cooperative rearrangement steps. A time step corresponds to the number of simulation steps after which an average of one attempt to move each bead was made. More details about the algorithm used are given elsewhere [16–18]. The simulation of this type is very efficient and allows, for example, to observe a system consisting of a large number of beads (e.g., 320 linear chains of length $N = 100$) within the time period by factor 10^6 longer than the relaxation time of a single bead, using a personal computer.

The model used consisted of $40 \times 20 \times 40$ up to $160 \times 40 \times 160$ beads in x-, y- and z-directions, respectively (up to *ca.* 10^6 beads). The repulsive walls were placed at $x = 0$ and

$x = x_{max} + 1$. We usually used asymmetric lattices with the x- and z-dimensions bigger. The x_{max} was made bigger because in this direction periodic boundary conditions were not applied and it should be by at least an order of magnitude bigger than the radius of gyration of the chain, to avoid strong confinement effects. The z-dimension was made big because the coil dimension in this direction increases even several times under shear flow. The chain length was $N = 4$, 10, 20, 40, 80, 160, 320 or 640. In order to generate initial equilibrium states, a dense system of chains was subjected to motion under athermal conditions for a time much longer than the chain relaxation time.

To reduce boundary effects the periodic boundary conditions have been employed in the y- and z-directions. The plane-parallel flowing system is asymmetric in the direction of the flow velocity gradient. Therefore we cannot use periodic boundary conditions in this direction (x-direction in our case) and we have to introduce two impenetrable walls (non-interacting, purely reflective in these simulations). Therefore the effect of the shear flow on molecular conformations and dynamics coexists with the effect of constrains brought about by the walls. Their relative importance, dependent on the distance from the wall, should be estimated.

In MC simulations a straightforward method of implementing a shear flow is an appropriate biasing of the probability of an individual bead move. It can be done in slightly different ways assuming that the total probability of move (averaged over all directions) is not changed by the shear flow. Pakula [11] used a simple biasing method, changing only relative probabilities in forward and backward directions, leaving probabilities in the perpendicular direction unchanged. In the model of Baschnagel and Binder [10] the biasing influences the probabilities in all directions. It makes possible simulation of a highly biased flow, increasing the probability of the jump in the flow direction at the expense of the Brownian movements in the transverse direction, which seems, however, not realistic under athermal conditions. The same method was used by Gleiman and Dorgan in their simulation of Poiseuille flow [12]. We compared both methods for the same system and found that for low and medium biasing the differences in the determined parameters and velocity profiles are of secondary importance so we used much more efficient and simpler bias algorithm of Pakula. As we shall demonstrate, in the case of polymer melt the bias profile between the walls is more important than the details of the biasing the individual bead move.

The shear flow was simulated by introducing biased probability of the bead movement in the z-direction. Since the coordination number is 12, there are four moves possible in the x–y plane (z-component equal to zero) and 8 with non-zero z-components (4 positive and 4 negative). Biasing was realized in such a way that the probability of the move in the x–y plane was left to be 1/12 in each direction while the probabilities of the moves with non-zero components in positive and negative z-directions were modified in such a way that the probability in that say positive direction $\boldsymbol{P}_{z^+}$ was increased by an amount of $\Delta\boldsymbol{P}$, while the probability of the move in the opposite direction $\boldsymbol{P}_{z^-}$ was decreased by $\Delta\boldsymbol{P}$ so that the total probability of the attempt to move in positive and negative directions was unchanged, equal to 8/12. To simulate the shear flow field in a plane-parallel geometry we introduced an x-dependent bias of the move probability so $\boldsymbol{P}_{z^+}$ was dependent on the maximum bias $\Delta\boldsymbol{P}_{max}$ and on the bead x-coordinate.

Two biasing profiles were used:

(i) bipolar – simulation of the case of two walls moving in the opposite directions with the same speed. Shear field is symmetrical with respect to $x = (x_{max} + 1)/2$ plane (the distance between the walls is equal to $x_{max} + 1$). In this case the probability bias depends on the distance from the $x = 0$ plane according to the formula:

$$\Delta\boldsymbol{P}_x = \Delta\boldsymbol{P}_{max}\left(\frac{x - 0.5(x_{max}+1)}{0.5(x_{max}-1)}\right)$$

so that the probability bias is equal to zero in the center and linearly increases to reach $\Delta\boldsymbol{P}_{max}$ for the move in the z-axis direction (+) for $x = x_{max}$ and $-\Delta\boldsymbol{P}_{max}$ for $x = 1$ (the move in the opposite direction (−)).

In this case

$$\boldsymbol{P}_{z^+}(x) = \frac{4}{12}(1 + \Delta\boldsymbol{P}_x) \quad \boldsymbol{P}_{z^-} = \frac{4}{12}(1 - \Delta\boldsymbol{P}_x)$$

hence the beads in the two halves of the system flow in the opposite directions.

(ii) unipolar – corresponding to one wall moving at a constant speed and the other being immobile. In this case the probability bias depends on the distance from the immobile $x = 0$ plane, according to the formula:

$$\boldsymbol{P}_{z^+}(x) = \frac{4}{12}\left(1 - \frac{x}{x_{max}}\Delta\boldsymbol{P}_{max}\right)$$

which means that the probability bias changes from weakly biased for $x = 1$ to fully biased ($\Delta\boldsymbol{P}_x = \Delta\boldsymbol{P}_{max}$) for $x = x_{max}$. All the beads in the system flow in the same direction.

In principle the two cases should be equivalent – they differ only by the coordinate system related to one of the walls or related to center of mass of the melt. In our simulations they really were at short times. Some differences were observed at long times and they are discussed below.

Four cases were simulated:

(0–0) – non-flowing melt, $\Delta\boldsymbol{P}_{max} = 0$ (for comparison with the flowing systems and as a starting point for the step-shear flow).

(0–f) – flow starting from the non-flowing equilibrated system (output of the case 0–0) (step-shear experiment – creep). Chain parameters at the beginning were the same as in non-flowing system. Some small average chain orientation was due to the presence of non-penetrable walls in the y–z planes.

(f–f) – equilibrium, steady-state shear flow – the simulations started from the system which reached equilibrium

under flow at the same bias (as monitored by the end-to-end vector autocorrelation function falling down to zero – output of the case 0–f or f–f). Chains were therefore preoriented accordingly for the $\Delta \boldsymbol{P}_{\max}$ used in this simulation. (f–0) – melt relaxation after flow (recovery). Initially the system was in an equilibrium shear flow with a given $\Delta \boldsymbol{P}_{\max}$ (output of the case 0–f or f–f) but the simulation was carried on with $\Delta \boldsymbol{P}_{\max} = 0$.

3. Quantities determined

Melt flow velocity $\boldsymbol{v}_x$ was monitored by calculating displacements of the beads in the flow direction during one simulation time step and averaging over a y–z layer having the same x-coordinate, thus the same probability bias.

In order to characterize chain conformation the following parameters were calculated: the average (root mean squared) end-to-end distance

$$R = \sqrt{\frac{1}{N_c}\sum_i (r_N - r_1)^2} \tag{1}$$

where $\boldsymbol{r}_N$ and $\boldsymbol{r}_1$ are space coordinates of monomers at chain ends, N is the number of monomers (beads) in the chain and N_c is the number of chains in the system.

The radius of gyration

$$R_g = \sqrt{\frac{1}{NN_c}\sum_n \sum_i (r_{i,n} - r_{cm,n})^2} \tag{2}$$

where $\boldsymbol{r}_{i,n}$ and $\boldsymbol{r}_{cm,n}$ are space coordinates of monomer i and of the center of mass of the n-th chain. The coil deformation in the flowing systems was monitored calculating average values of x, y and z components of these parameters ($\boldsymbol{R}_x$, $\boldsymbol{R}_y$, $\boldsymbol{R}_z$, $\boldsymbol{R}_{g_x}$, $\boldsymbol{R}_{g_y}$, and $\boldsymbol{R}_{g_z}$). In this case in the above formulae three-dimensional space coordinates $\boldsymbol{r}_{i,n}$, $\boldsymbol{r}_{cm,n}$ were replaced by their x, y or z coordinates, respectively.

In some cases, when the position dependence of a given parameter was investigated, the averaging was performed over the ensemble of chains for which the centers of mass were in a given y–z layer. In the equilibrium case additional averaging was performed over states of the system sampled in constant time intervals Δt, being of the order of the chain relaxation time.

The orientation of $\boldsymbol{R}$ with respect to flow direction was characterized by the orientation factor:

$$f_R = \frac{1}{2}\left(3\langle \cos^2 \theta_R \rangle - 1\right) \tag{3}$$

where θ_R is the angle between the end-to-end vector and the z-axis and the averaging is performed over end-to-end vectors of all the chains in the system.

Local chain orientation $\boldsymbol{f}_L$ was characterized using not simply a bond orientation (orientation of the vector connecting two adjacent beads) but by a two-bond vector orientation factor (orientation of the vector connecting a given bead with its second next neighbor, i.e., n and $n+2$, with respect to the flow direction):

$$f_L = \frac{1}{2}\left(3\langle \cos^2 \theta_{2B} \rangle - 1\right) \tag{4}$$

We found it more informative because on the fcc lattice an average single bond orientation is the same for an extended zigzag chain oriented along the x-, y- or z-axis thus two-bond vector is the smallest unit which carries information on the local chain orientation.

In order to get information about the dynamic properties of the investigated systems the following quantities were monitored in time:

(1) The end-to-end vector autocorrelation function

$$\rho_R(t) = \frac{1}{N}\sum_N R(0)\cdot R(t) \tag{5}$$

where $\boldsymbol{R}(0)$ and $\boldsymbol{R}(t)$ denote end-to-end vectors at time $t = 0$ and t, respectively.

The above correlation function was used to determine relaxation times τ by fitting a sum of stretched exponential functions

$$\rho_{fit}(t) = \sum_i A_i \exp\left[-\left(\frac{t}{\tau_i}\right)^{\beta_i}\right] \tag{6}$$

where the number of component i was 1 or 2.

(2) Mean-square displacements of monomers and of centers of mass of the chains:

$$r_m^2 = \frac{1}{NN_c}\sum_{N_c}\sum_N \left[r_i(t) - r_i(0)\right]^2 \tag{7}$$

$$r_{cm}^2 = \frac{1}{N}\sum_N \left[r_{cm,j}(t) - r_{cm,j}(0)\right]^2 \tag{8}$$

where $\boldsymbol{r}_i(t)$, $\boldsymbol{r}_{cm,j}(t)$, $\boldsymbol{r}_i(0)$, $\boldsymbol{r}_{cm,j}(0)$ are monomer and chain center of mass coordinates at time t and $t = 0$, respectively.

4. Results and discussion

4.1. Non-flowing polymer melts between neutral walls – case (0–0)

Results obtained for the non-flowing systems (Figs. 1 and 2) are very similar to those reported previously for the polymer melt between reflective impenetrable walls with periodic boundary conditions in y- and z-directions [21,22] (with regard to the parameters averaged over all the system) and also for the systems with periodic boundary conditions in three dimensions [23]. In particular the system-averaged $\boldsymbol{R}^2$ and $\boldsymbol{R}_g^2$ scale with the chain length N, in agreement with theoretical predictions ($\boldsymbol{R}^2$, $\boldsymbol{R}_g^2 \sim N$). Close to the walls the chains are oriented with $\boldsymbol{R}$ parallel to the walls, which results in a decrease of

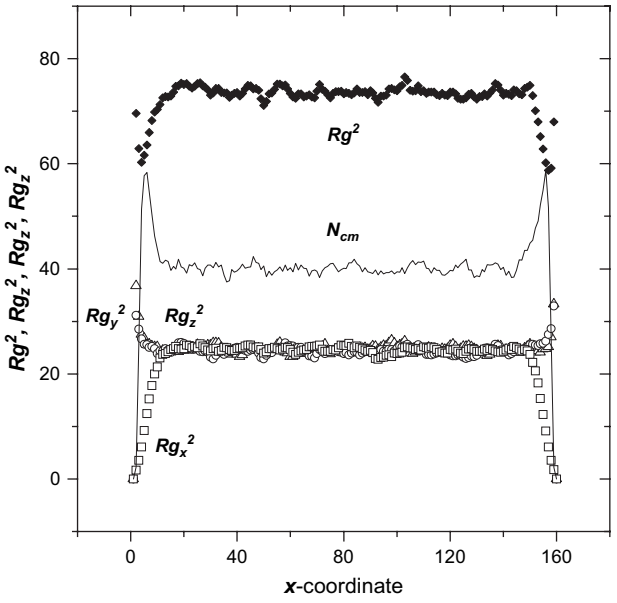

Fig. 1. Dependence of the radius of gyration $\boldsymbol{R}_g$ and its components $\boldsymbol{R}_{g_x}$, $\boldsymbol{R}_{g_y}$, $\boldsymbol{R}_{g_z}$ on the chain center of mass position with respect to the walls in the non-flowing system (case 0–0), $N = 160$. Solid line shows the corresponding distribution of the center of mass density.

$\boldsymbol{R}_{g_x}$ and an increase of $\boldsymbol{R}_{g_y}$ and $\boldsymbol{R}_{g_z}$ of the chains with the center of mass located near the wall (solid line in Fig. 1).

Chain dynamics is also very similar to the dynamics in the bulk as illustrated in Fig. 2. It is characterized by the end-to-end vector autocorrelation function $\boldsymbol{\rho_R}$ which can be approximated by the stretched exponential function (Eq. (6) with $i = 1$). The parameter $\boldsymbol{\beta}$ decreases with increasing chain length. The chain relaxation time dependence on N indicates an onset of the entanglement effects ($\boldsymbol{\tau} \sim N^{\alpha}$ with $\alpha > 3$) [1–4] for the longest simulated chains ($N > 160$).

4.2. Steady-state shear flow of the melts – case (f–f)

Fig. 3 presents flow velocity profiles between the walls for different chain lengths N, under constant $\Delta\boldsymbol{P}_{\max} = 0.8$, i.e., for the strongly biased move probability. The profiles have chain length dependent slopes and linearities. The velocity gradients decrease with the increasing chain length. The range in which the profiles are linear also decreases.

The effect of $\Delta\boldsymbol{P}_{\max}$ on normalized velocity profiles $\boldsymbol{v}_{(x)}/\Delta\boldsymbol{P}_{\max}$ is shown in Fig. 4 for the chains of length $N = 160$, for the bipolar bias. The unipolar bias gives almost identical results, in particular where $\Delta\boldsymbol{P}_x$ approaches zero (it means that near ''immobile wall'') the flow is not significantly affected. It can be seen that the flow profile is nearly linear only for small $\Delta\boldsymbol{P}_{\max}$ but becomes strongly nonlinear for high $\Delta\boldsymbol{P}_{\max}$. Non-Newtonian flow close to the ''moving'' walls can be explained by the effect of spatial constraint near the walls, leading to restricted mobility and different conformations of the chains adjacent to the wall or being very close to it [21,22]. The restricted mobility has stronger effect on quickly flowing chains (high probability bias) and on long chains having more beads in contact with the plane. However, it should be noted that the direct effect of the wall does not depend strongly on the chain length and it can be clearly seen only in the 5–8 layers adjacent to the wall. For these layers the velocity gradient can even change sign (see Fig. 3, chains of $N > 80$ and Fig. 4). This effect is probably still underestimated since the MD simulations of Aoyagi et al. [24] show that the layers adjacent to the walls are additionally compressed towards the walls, which should further reduce the molecular mobility.

Nonlinear effects observed in Figs. 3 and 4 cannot be related only to the presence of the walls since they are also observed near the center. In this region $\Delta\boldsymbol{P}_x$ approaches zero but the velocities exceed extrapolated linear values, which result

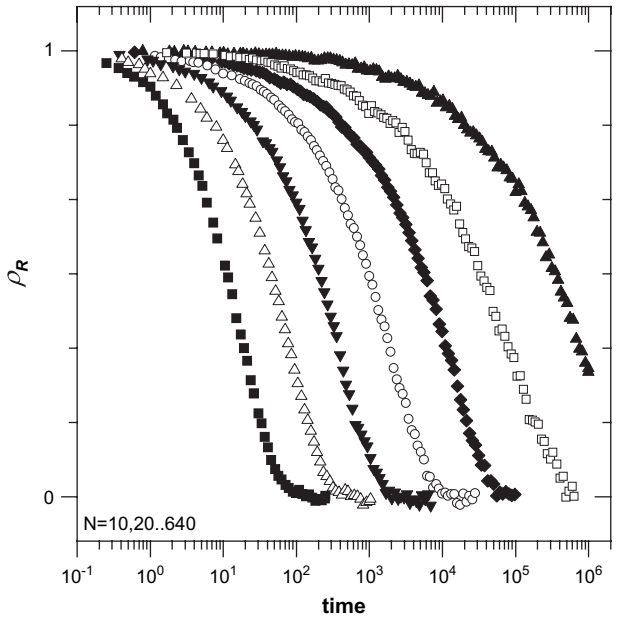

Fig. 2. End-to-end autocorrelation functions $\boldsymbol{\rho_R}$ in the non-flowing system (case 0–0) for various chain lengths ($N = 10$, 20, 40, 80, 160, 320 and 640).

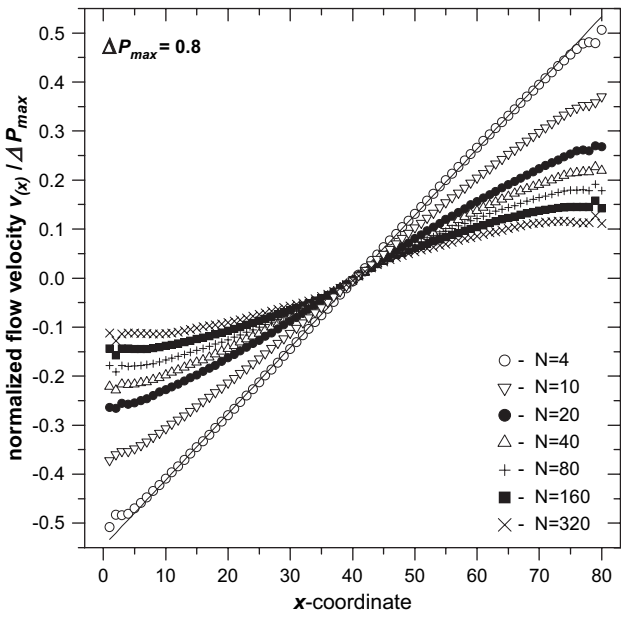

Fig. 3. Position dependence of the layer-averaged flow velocities $\boldsymbol{v}_x$ for different chain lengths ($N = 4$, 20, 40, 80, 160 and 320). $\Delta\boldsymbol{P}_{\max} = 0.8$.

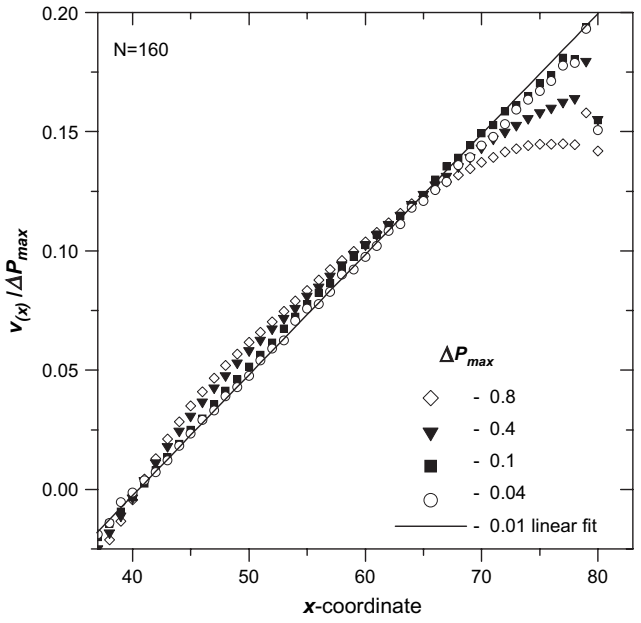

Fig. 4. Position dependence of layer-averaged flow velocities obtained for different ΔP_{max}, normalized by dividing by ΔP_{max}. Chain length $N = 160$. For clarity only the part of the system in which the melt flows in the positive direction is presented (case f–f).

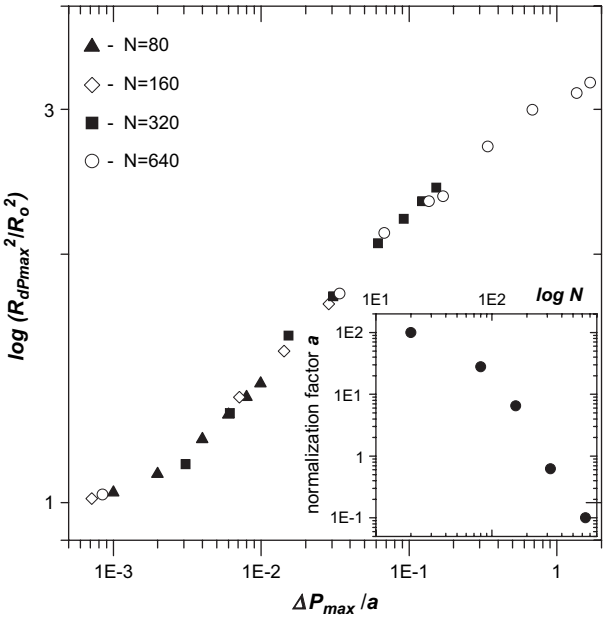

Fig. 5. Increase of the normalized mean square end-to-end vector R^2 under flow. The plots for different chain lengths are shifted along the ΔP_{max} scale to show the master curve. The inset shows shift factors for various chain lengths.

in the velocity gradient much higher than the average value, increasing with increasing chain length. It is true both for bipolar and unipolar biases, although in the latter case the wall effect dominates in the adjacent 6–8 layers (not shown here, but cf. Fig. 6). Nonlinearity far from the walls is probably related to the fact that different parts of a chain are subjected to different biases but their flow must be correlated to some extent to preserve the chain continuity. We are aware of the fact that nonlinear velocity profile implies that the shear gradient should also be nonlinear, which in turn will modify the velocity profiles (in a different way, depending on ΔP_{max} and N). Thus the presented results provide a qualitative picture of the real situation. However, it should be expected that the appropriate correction will not be big and that the flow will remain nonlinear. We performed some simulations using nonlinear bias profiles, even such for which linear velocity profiles for long chains were obtained. Such corrections do not influence significantly the system-averaged values of the parameters considered in the rest of this paper.

In flowing melts one can observe coil deformation and orientation of the end-to-end vector in the flow direction. This effect is stronger if higher is the stress and longer is the chain. The orientation effects become strong for high ΔP_{max} and for long chains as should be expected. For long chains some orientation is observed also in the non-flowing system ($\Delta P_{max} = 0$), due to the orientation of the chain end-to-end vector near the walls as a result of the space confinement, as shown in Ref. [21]. This effect becomes stronger with decreasing ratio between R_g and the distance between the walls.

Fig. 5 shows the increase of R^2 under shear. The chain extension is proportional to the increase of the free energy of the system and it becomes important for longer chains even at low probability bias. The results are presented as the dependence of the normalized average squared end-to-end distance R^2/R_0^2 on ΔP_{max} in double logarithmic coordinates (R_0^2 is the corresponding value in the non-flowing melt). The sets of values obtained for a given N are scaled using $\Delta P_{max}/a$ coordinate (which corresponds to a shift by a along the ΔP_{max} scale) to obtain a master curve. The master curve and the shift factor dependence on N are qualitatively similar to those obtained in Ref. [25] for the Rouse chain in solution. The direct comparison cannot be made because these authors use the longest Rouse relaxation times and shear rate (not shear stress) in their reduced coordinate system. Strict correspondence is also not to be expected as our longest chains are above the crossover to the entanglement regime. Similar results were obtained for R_g in this work and in Ref. [25]. In the athermal case, corresponding to high temperature, we could not obtain significant extension and alignment of short chains under flow as in Refs. [6–8]. These effects are, however, clearly observed for longer chains ($N = 80$–640).

The coil deformation in the flowing system is, however, not uniform and it depends on the position of the center of mass with respect to the walls. Fig. 6 presents the dependence of $R_{g_z}^2$ of the chains on the x-coordinate of their center of mass for various probability biases. Generally all the chains are the more extended the higher is ΔP_{max}. For a given ΔP_{max} their $R_{g_z}^2$ increases with decreasing distance from the walls, i.e., where they experience higher probability bias and where they flow faster. Only in the close vicinity of the wall (6–8 layers) where their mobility is reduced, a slight decrease is observed for big ΔP_{max}. The solid line shows the R_{g_z} dependence in the case of unipolar flow with the same bias profile as in a half of the bipolar system. It can be seen that it is almost

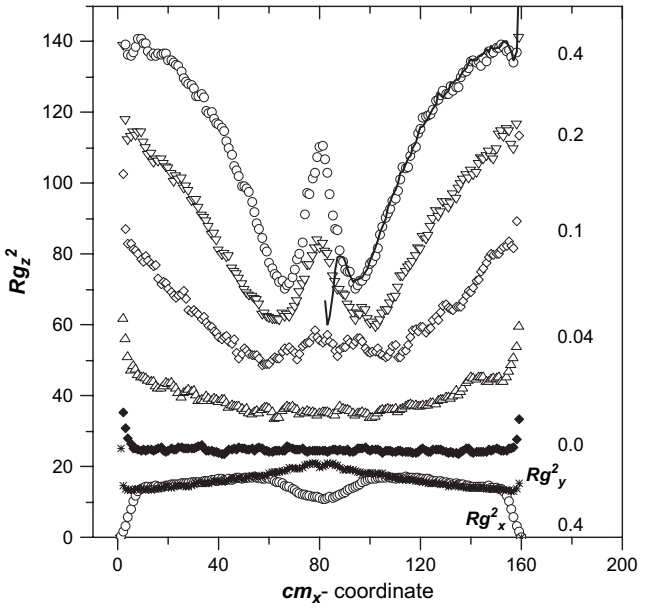

Fig. 6. Dependence of the z-component of the radius of gyration $\boldsymbol{R}_{g_z}$ on the chain center of mass position with respect to the walls in the steady-state flowing system (case f–f) for various probability biases $\Delta\boldsymbol{P}_{max}$ (indicated in the figure). Bipolar flow, $N = 160$. The components $\boldsymbol{R}_{g_x}$, $\boldsymbol{R}_{g_y}$, for $\Delta\boldsymbol{P}_{max} = 0.4$ and for $\Delta\boldsymbol{P}_{max} = 0$ are also shown. The solid line shows the same dependence for the unipolar bias case, corresponding to a half of the bipolar system. The data for the unipolar bias are shifted by 80 units along the x-axis to allow easier comparison of the two cases.

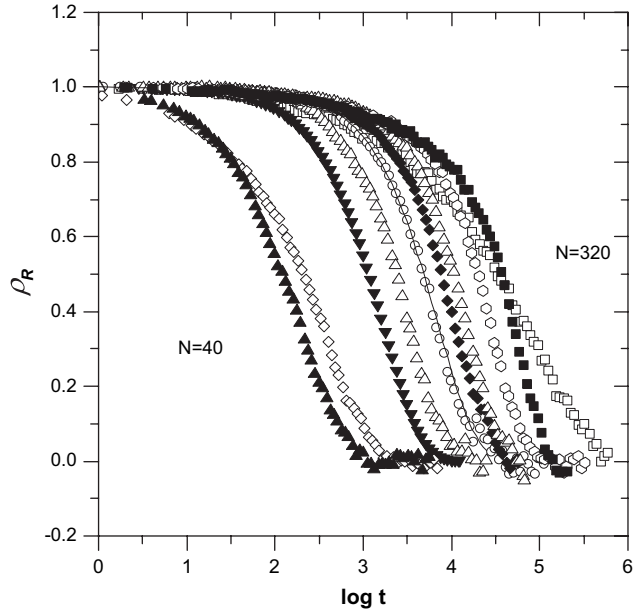

Fig. 7. End-to-end autocorrelation functions $\boldsymbol{\rho}_{\boldsymbol{R}}$ in the flowing system (case f–f) for chains $N = 320$ and $N = 40$ for various probability biases. For $N = 320$, $\Delta\boldsymbol{P}_{max} = 0.8$, 0.4, 0.2, 0.1, 0.08, 0.04 0.01 and 0.001 and for $N = 40$, $\Delta\boldsymbol{P}_{max} = 0.8$ and 0.01 (form the left to the right). The solid line shows fitting using a single stretched exponential.

identical except very close to the wall at which $\Delta\boldsymbol{P}_x = 0$. Some increase at low $\Delta\boldsymbol{P}_x$ is observed, similar to that in the center of the bipolar system, but it is apparently overcome by the decrease of mobility close to the wall. $\boldsymbol{R}^2_{g_x}$ and $\boldsymbol{R}^2_{g_y}$ components decrease under shear as compared with the values in the (0–0) case also shown for comparison (full diamonds). $\boldsymbol{R}^2_{g_x}$ (but not $\boldsymbol{R}^2_{g_y}$) shows a minimum in the very center, corresponding to an anomalous maximum of $\boldsymbol{R}^2_{g_z}$. It suggests that this maximum is related to high velocity gradient in this range (Figs. 3 and 4) due to nonlinear flow.

Fig. 7 shows the end-to-end vector autocorrelation functions for $N = 40$ and for $N = 320$ for various probability biases and in the non-flowing systems. Chain relaxation is generally faster under shear. In the case of long chains it is strongly dependent on $\Delta\boldsymbol{P}_{max}$, even in weakly biased systems. For short chains ($N = 40$) the difference between the relaxation in the non-flowing and quickly flowing systems ($\Delta\boldsymbol{P}_{max} = 0.8$) is small, while for long chains ($N = 320$) this difference is very important even for $\Delta\boldsymbol{P}_{max} = 0.04$. Long chain relaxation in the equilibrated flowing system follows quite well the stretched exponential law (Eq. (7) with $i = 1$) with $\boldsymbol{\beta} = 0.85$ (as shown by the solid line in Fig. 7) until $\Delta\boldsymbol{P}_{max}$ is not too small. For $\Delta\boldsymbol{P}_{max} < 0.08$ using Eq. (7) with $i = 2$ is necessary to obtain good fitting, and the $\boldsymbol{\beta}_2$ coefficient corresponding to longer relaxation time is equal to 1. The results for $\Delta\boldsymbol{P}_{max} = 0.001$ are practically identical with those for the non-flowing melt and show quite a different time dependence from those for $\Delta\boldsymbol{P}_{max} = 0.02$, although the half-times are practically equal. This surprising crossover phenomenon needs further studies.

Fig. 8 presents the time dependence of $\boldsymbol{\rho}_{\boldsymbol{R}}$ for various chain lengths under medium shear ($\Delta\boldsymbol{P}_{max} = 0.1$). Comparing with Fig. 2 for the (0–0) case it is worth to note that the differences between the relaxation times of long chains become smaller under shear and their slopes are significantly bigger (the $\boldsymbol{\beta}$ coefficient in the stretched exponential function increases e.g. for $N = 640$ from *ca.* 0.5 to 1). In Fig. 9 the longest relaxation times $\boldsymbol{\tau}$ for all the simulated systems are plotted vs. $\Delta\boldsymbol{P}_{max}$. For the

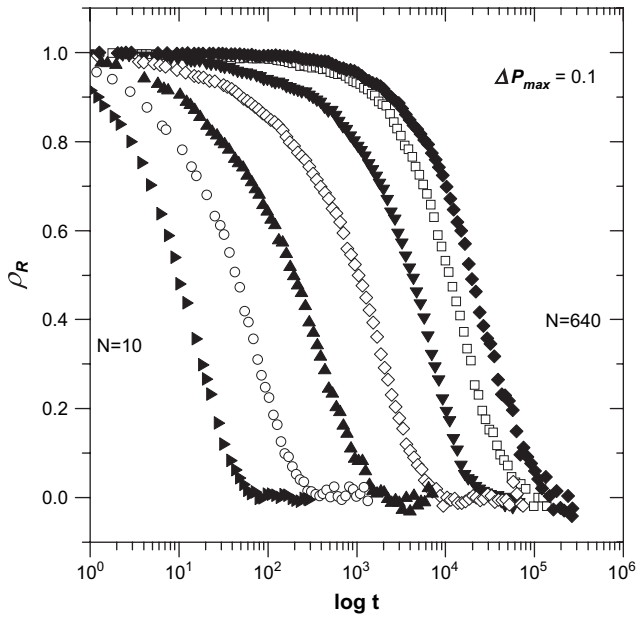

Fig. 8. End-to-end autocorrelation functions $\boldsymbol{\rho}_{\boldsymbol{R}}$ in the flowing system (case f–f) for various chain lengths $N = 10$, 20, 40, 80, 160, 320 and 640 (from the left to the right). Probability bias $\Delta\boldsymbol{P}_{max} = 0.1$.

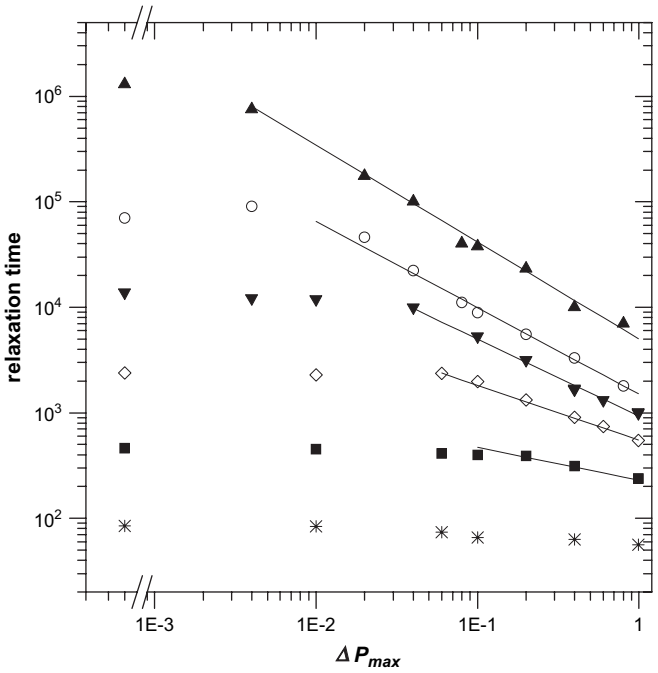

Fig. 9. Relaxation times of the dominant (slower) relaxation process in the flowing polymer melt plotted vs. $\Delta \boldsymbol{P}_{\max}$ for different chain lengths ($N = 20$, 40, 80, 160, 320 and 640, from the bottom up). Corresponding values for the non-flowing systems (zero-shear values) are shown on the left of the axis brake.

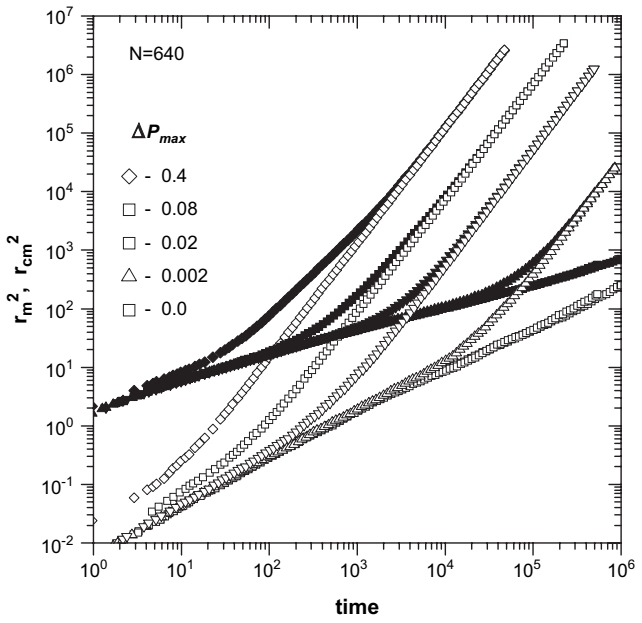

Fig. 10. Mean-square displacement of beads (full symbols) and centers of mass (empty symbols) of the chains $N = 640$ in the flowing melt (case f–f) for various shear stresses.

short chains the $\boldsymbol{\tau}$ dependence on $\Delta \boldsymbol{P}_{\max}$ is weak, while for the longest chains studied $\boldsymbol{\tau}$ decreases by nearly 2 orders of magnitude for high shear stress. This effect corresponds to the well-known shear thinning of polymer liquids, described by the power law relating viscosity to shear rate: $\eta \sim \dot{\gamma}^{n-1}$ [1,2,26]. In our case it takes a form $\tau \sim \Delta \boldsymbol{P}_{\max}^{n-1}$ with $n = 1.92$, 1.82, 1.73 and 1.52 for $N = 640$, 320, 160 and 80, respectively (solid lines). For shorter chains the power law applies in a narrow range of highest $\Delta \boldsymbol{P}_{\max}$ which also corresponds to experimental findings [1,2,26].

The time dependence of average square displacements of the beads $\boldsymbol{r}_m^2$ and chains $\boldsymbol{r}_{\mathrm{cm}}^2$ in the flowing melt is presented in Fig. 10 (chains of $N = 640$). For so long chains practically all the investigated time range correspond to a transition range between $\boldsymbol{r}_m^2 \sim t$ (for very short times) and the long time regime (Fickian), where again $\boldsymbol{r}_m^2$ and $\boldsymbol{r}_{\mathrm{cm}}^2 \sim t$. For the non-flowing melt (also shown) $\boldsymbol{r}_m^2 \sim t^{0.42}$ and $\boldsymbol{r}_{\mathrm{cm}}^2 \sim t^{0.75}$. Both exponents are smaller than those expected for Rouse chains (0.5 and 1, respectively). The exponents increase with decreasing N to reach the predicted values for chains below $N = 40$ (cf. Fig. 18 below). Even for $N = 640$ these coefficients are, however, bigger than those predicted by the reptation model (0.25 and 0.5, respectively [26]). It suggests that although entanglements are important in our system, we are still in a broad crossover range from the Rouse regime to the reptation regime [27]. It should also be noted that the reptation model assumes immobile obstacles and only in such a case so low slopes were obtained in simulations [28,29]. The different slopes can also be related in part to an asymmetry of diffusion due to confinement between the walls (vide infra). In the flowing melt, at times longer than the corresponding relaxation time, both $\boldsymbol{r}_m^2$ and $\boldsymbol{r}_{\mathrm{cm}}^2$ increase as t^2, i.e., the shear-induced displacement dominates. The increase of the slope begins at longer time when $\Delta \boldsymbol{P}_{\max}$ is smaller, in accordance with the increase of the relaxation time (Fig. 9). For very small bias (below 0.01) clear observation of the t^2 dependence requires unreasonably long simulation time. For sufficiently quickly flowing melts (small N and/or big $\Delta \boldsymbol{P}_{\max}$) one can independently determine $\boldsymbol{v}_z$ from the linear part of the $\boldsymbol{r}_{\mathrm{cm}}^2$ dependences at long times, especially for the unipolar biasing (vide infra) in good agreement with the local velocities shown in Figs. 3 and 4 (when averaged over a half of the system).

4.3. Step-shear and melt recovery

Evolution of the end-to-end vector $\boldsymbol{R}$ and of z- and y-components of $\boldsymbol{R}_{\mathrm{g}}$ in time (case 0–f) for different $\Delta \boldsymbol{P}_{\max}$ is shown in Fig. 11. The coil deformation brings about an increase of the z-components while y- and x-components decrease in the flowing system. That is why for $\Delta \boldsymbol{P}_{\max} = 0.4$ $\boldsymbol{R}_z^2$ increases almost 4 times while $\boldsymbol{R}^2$ increases less than twice. For $x_{\max} < 40$ and $N > 80$ a difference in $\boldsymbol{R}_{\mathrm{g}}$ components is observed also in non-flowing systems. $\boldsymbol{R}_{\mathrm{g}_y}$ and $\boldsymbol{R}_{\mathrm{g}_z}$ are equal but the $\boldsymbol{R}_{\mathrm{g}_x}$ is smaller due to the space confinement near the walls (Fig. 1). The coil deformation increases with increasing $\Delta \boldsymbol{P}_{\max}$ but the time dependence is similar for different $\Delta \boldsymbol{P}_{\max}$. However, the onset of the deformation depends strongly on $\Delta \boldsymbol{P}_{\max}$. Interestingly the contraction in the x- and y-directions begins *ca.* 3 times later than its extension, and it continues when the extension is already accomplished (see vertical line in Fig. 11b). The time dependences of chain extension in the flow direction and contraction in perpendicular directions are different because the extension in the z-direction is caused by the stress

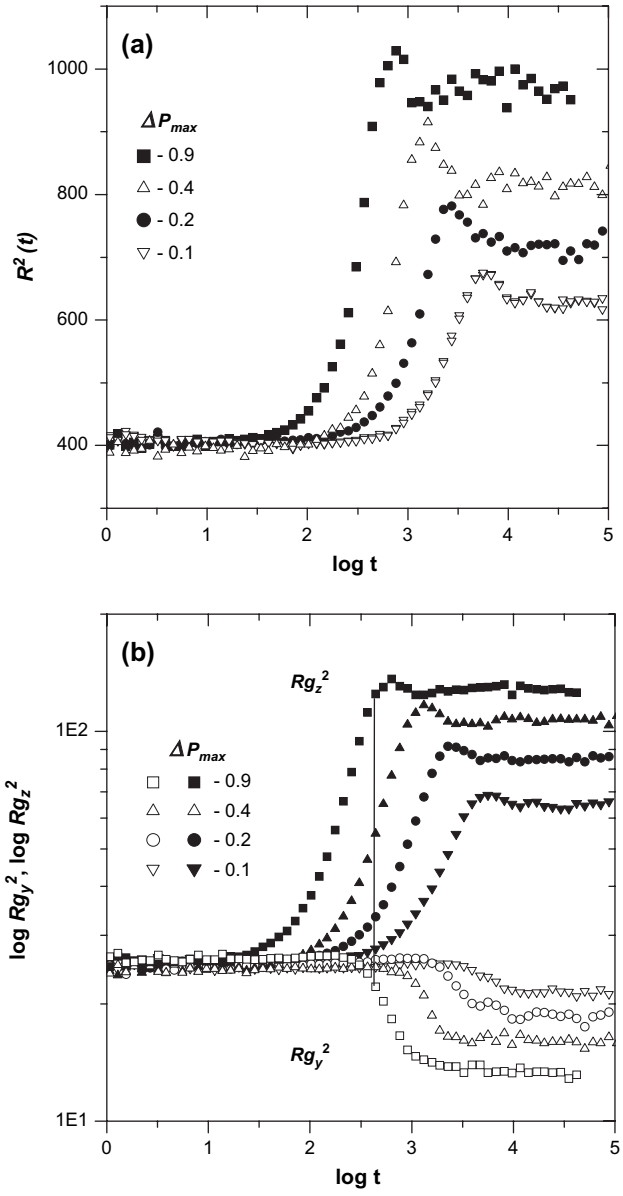

Fig. 11. Time dependence of $\boldsymbol{R}^2$ (a) and z- and y-components of $\boldsymbol{R}_g^2$ (b) in the simulation of the step-shear experiment (case 0–f) for $\Delta\boldsymbol{P}_{max} = 0.8$, 0.4, 0.2, 0.1. Chain length $N = 160$. Vertical line is drawn to make easier the comparison of the time dependence of the two $\boldsymbol{R}_g$ components.

so it is fast, while the contraction in x- and y-directions is of "entropic" origin thus it is slow. An analogous difference between kinetics of chain extension in the 0–f case and contraction (f–0 case) is shown below (Fig. 13)

In Fig. 11 it can be seen that in the case of flow of non-pre-oriented systems (case 0–f) the increase of $\boldsymbol{R}_g$ and $\boldsymbol{R}$ shows an "overshoot" – they initially increase above the equilibrium value. Similar effects were observed also in other simulations of polymer melts [12,30–32], for single chains in solutions [33] and in the time dependence of strain in the creep experiment e.g. Refs. [1,34]. A similar overshoot of the chain orientation factor is not observed (Fig. 12).

In Fig. 12 the time dependence of local ($\boldsymbol{f_L}$) and chain ($\boldsymbol{f_R}$) orientation factors is presented. An increase of the local, two-bond orientation begins earlier than the end-to-end vector

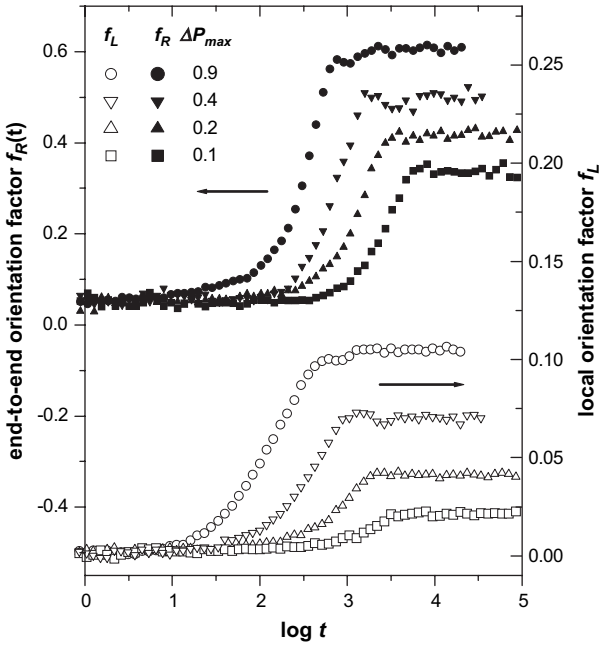

Fig. 12. Comparison of the time dependence of the end-to-end vector orientation factor $\boldsymbol{f_R}$ and the local (two-bond) orientation factor $\boldsymbol{f_L}$ in the (0–f) case for various $\Delta\boldsymbol{P}_{max} = 0.8$, 0.4, 0.2, 0.1. Chain length $N = 160$.

orientation, which follows approximately the chain extension kinetics (compare Fig. 11). However, as it increases faster, the steady-state values are reached approximately at the same time. It is interesting to note that both $\boldsymbol{f_L}$ and $\boldsymbol{f_R}$ begin to increase not at the same time for various shear stresses, as one could expect, but the later the smaller is $\Delta\boldsymbol{P}_{max}$. The chains need also much less time to reach higher orientation under higher stress. It means that an increase of molecular mobility under stress is much more important from the point of view of kinetics than the bigger degree of coil rearrangement under bigger stress.

The time dependence of the end-to-end vector autocorrelation function in the step-shear simulation (0–f) case) for two chain lengths ($N = 40$ and 320) and various $\Delta\boldsymbol{P}_{max}$ is shown in Fig. 13. It can be seen that for $N = 40$ at $\Delta\boldsymbol{P}_{max} = 0.1$ the chain relaxation is already close to the relaxation in the non-flowing system, while for $N = 320$ the difference between the flowing and non-flowing systems is significant also for very small $\Delta\boldsymbol{P}_{max}$ (below 0.05). The chain relaxation is close to that of the non-flowing system for some time (the longer the smaller is $\Delta\boldsymbol{P}_{max}$) and then it decreases very fast. Even for small $\Delta\boldsymbol{P}_{max}$ the autocorrelation function falls down abruptly, but it takes place after longer time.

The chain relaxation in the two non-flowing systems (0–0) (Fig. 1) and (f–0) is practically identical, independent on chain length, while in the systems subjected to shear, (f–f) and (0–f) it is generally much faster. In spite of the different time dependencies in the (0–f) and (f–f) cases (Figs. 7 and 13) the corresponding half-times are very similar. The differences in dynamics in the four cases considered are strongly dependent on chain length – for short chains the cases (0–f) and (f–f) are very similar and the differences between them (and the (0–0) and (f–0) cases) are also small, while for long chains the differences are important even for $\Delta\boldsymbol{P}_{max} = 0.1$.

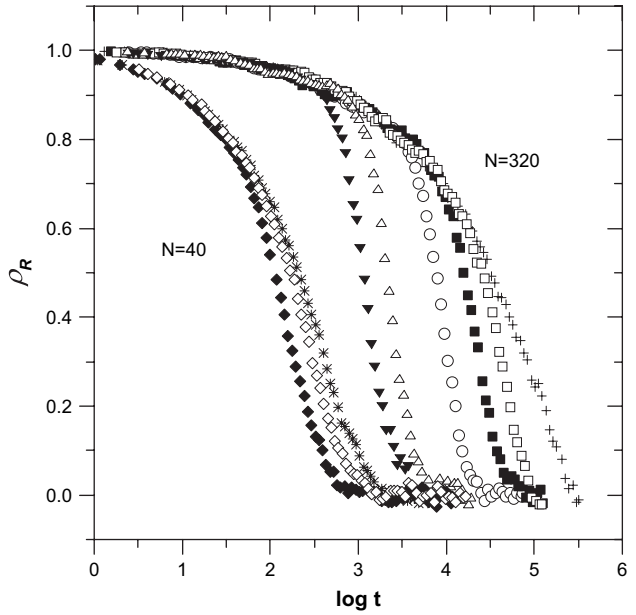

Fig. 13. End-to-end vector autocorrelation function for various ΔP_{max} for chain lengths $N = 40$ and $N = 320$. Case 0–f. For $N = 40$, $\Delta P_{max} = 0.8$, 0.1 and 0.0, for $N = 320$, $\Delta P_{max} = 0.8$, 0.4, 0.1, 0.04, 0.02 and 0.001.

A comparison of the time dependence of various parameters during creep and recovery is shown in Fig. 14. The local orientation (empty triangles) increases faster in the (0–f) case than it relaxes after the strain has been removed (f–0 case) but the half-time is the same in the two cases. By contrast, the chain orientation (lines) increases much faster in the (0–f) case than it relaxes in the (f–0) case. It concerns both the time range in which the relaxation takes place and the half-time, which is 30 times longer in the (f–0) case. The rapid decrease of ρ_R in the (0–f) case can be related to the increase of chain extension and orientation under shear. It is interesting to note that the chain relaxation in the step-shear simulation (0–f case) is slow, very similar to that of the non-flowing system, until the chain orientation becomes important (c.f. full squares, full circles and starred line). It can also be seen that the rapid relaxation should not be related to the local chain orientation (down triangles) but rather to the end-to-end vector orientation that starts later but increases faster. Evolution of chain orientation in time is somewhat slower than the end-to-end relaxation (c.f. solid line and full circles).

Fig. 15 shows time dependencies of the mean-square displacements of beads r_m^2 and chains r_{cm}^2 as well as their x-, y- and z-components $\left(x_m^2, y_m^2, \ldots, z_{cm}^2\right)$ in the step-shear case (0–f) and in the non-flowing melt (case 0–0). It can be seen that in the flowing system at longer times the total bead and chain displacements are dominated by the z-component (in the flow direction), thus the influence of shear stress on mobility cannot be analyzed in detail on the basis of r_{cm}^2 and only an analysis of its components provides valuable information. It is worth to note that z_{cm}^2 does not follow t^2 law in a broad time range, as it was observed in the (f–f) case (compare Fig. 10) but clearly shows $t^{1.75}$ time dependence over 2.5 decades before the relaxation time ($\tau \approx 10^4$) is reached. The x- and y-components (triangles) are almost identical, except for a small difference for very long times, the origin of which will be discussed later on. They are, however, significantly different from the corresponding values for the non-flowing melt (crosses). In the short time range x_m^2 and y_m^2 depend on time following $t^{0.5}$ law, as predicted by the Rouse model in the intermediate regime, while x_{cm}^2 and y_{cm}^2 follow $t^{0.75}$ law. However, above around $t = 10^3$ they

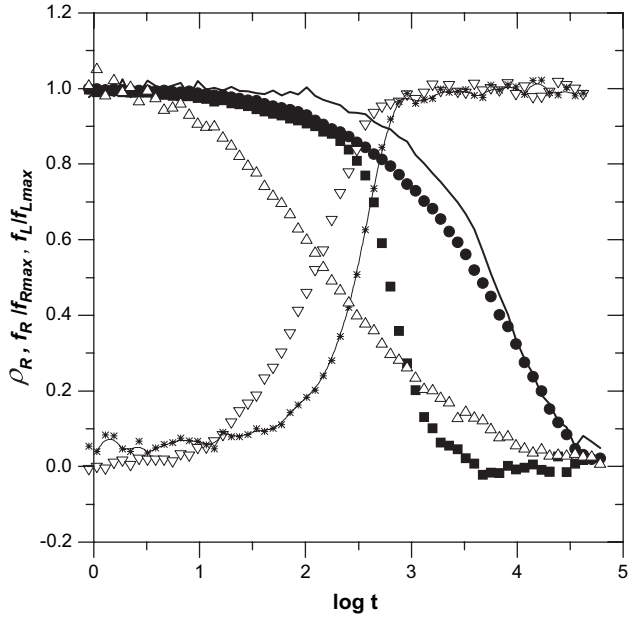

Fig. 14. Comparison of time dependences of various parameters characterizing chain dynamics in the creep and melt relaxation simulations (0–f and f–0 cases). Local orientation – empty triangles, chain orientation – lines and chain autocorrelation functions – full symbols. $N = 160$, $\Delta P_{max} = 0.8$. See text for details.

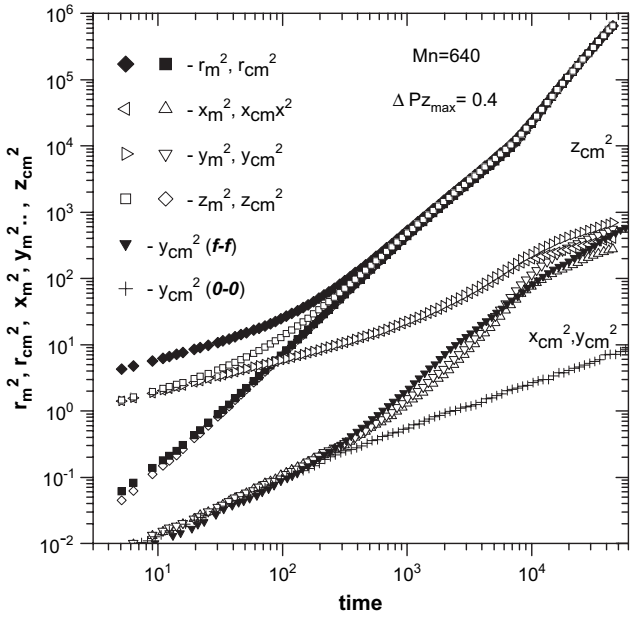

Fig. 15. Mean-square displacement of beads and centers of mass as well as their x-, y-, and z-components in the simulation of creep experiment (case 0–f). $\Delta P_{max} = 0.4$, $N = 640$. The y-components of r_{cm}^2 in the cases (0–0) and (f–f) are also shown for comparison.

begin to increase faster and above $t \approx 10^4$ follow again $t^{0.75}$ time dependence. It means that the coil deformation and orientation, which take place in this time range, is accompanied by an increase in chain and bead mobilities in all directions. It is not surprising that in the flowing systems (f–f) (Fig. 10) and (0–f) (Fig. 15) the displacements in the flow direction is bigger as compared with the (0–0) (f–0) cases. It is, however, interesting to note that the probability bias in the z-direction increases significantly also the molecular mobility in the perpendicular directions, in particular the x_{cm}^2 and y_{cm}^2 components (compare triangles and crosses in Fig. 15). A small difference in the time dependence between cases (f–f) (full down triangles) and (0–f) (empty down triangles) manifests only as a more or less rapid increase around the relaxation time.

In principle the time dependence of y_{cm}^2 should show $t^{1.0}$ dependence because in this direction we should not expect neither effect of space confinement, nor an effect of probability bias. It is, however, not the case. Exponents bigger or smaller than one mean that we observe an anomalous diffusion. In short and long time ranges we observe subdiffusion (exponent equal to 0.75 – smaller than one as discussed before) but in the intermediate range we observe superdiffusion (exponent equal to *ca.* 1.75 – much bigger than one). These effects also depend on the chain length (see below Fig. 18) but a detailed analysis is beyond the scope of this paper.

Most probably the anomalous diffusion is the result of a nonsymmetric bead move probability. It is evidently asymmetric in z- and x-directions, however, in the y-direction, where no asymmetry is introduced it is not so obvious. It can be presumed that the origin of the anomalous diffusion in this case is a broad distribution of ''waiting times'', which arises from the chain diffusion in the x-direction. The chain experiences different bias depending on the distance from the wall. It does not change the probabilities of the displacement to neighbor sites in the x- and y-directions, however, it changes the probability of closing the loop of the cooperative move.

4.4. Effects of walls spacing and biasing profile

The effect of confined space on chain dynamics was studied by changing wall spacing. The effect of confinement on the chain autocorrelation functions $\boldsymbol{\rho_R}$ in the cases (0–f) and (0–0) is shown in Fig. 16. In the non-flowing melt the wall spacing in the investigated range (40–160 layers) has a negligible influence on the chain relaxation (Fig. 16, rectangles), it becomes, however, important in the flowing system. It can be seen that in the 0–f case the effect of decreasing x_{max} is twofold: the chain relaxation is generally faster (relaxation time decreases 2.5 times) and the relaxation at longer times becomes faster.

Even more spectacular is the difference in the time dependence of $\boldsymbol{R}$ shown in Fig. 17. The increase of the end-to-end distance in the flowing system not only starts earlier if the wall spacing is smaller (in agreement with the decreasing relaxation time), but its steady-state values (indicated by the solid lines in Fig. 17) are also considerably smaller. Moreover the overshoot is more pronounced and relaxes faster in confined space. It

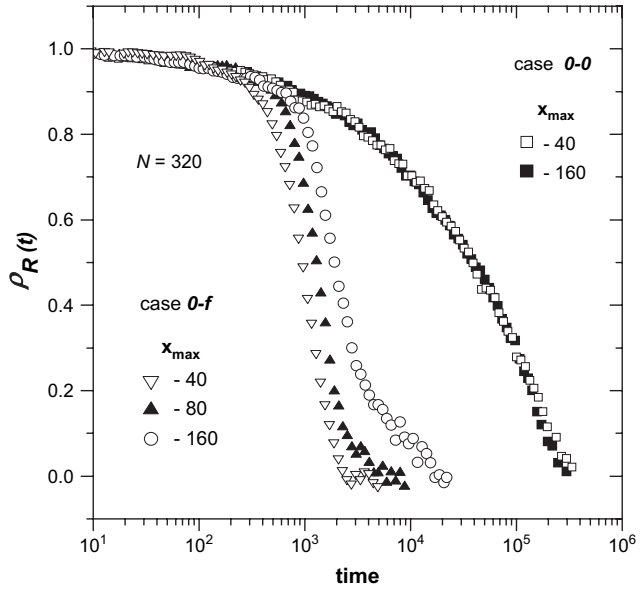

Fig. 16. End-to-end vector autocorrelation function for different x_{max} in non-flowing (0–0 case) and flowing melts (0–f case). $N = 320$, bipolar flow, $\Delta \boldsymbol{P}_{max} = 0.8$.

suggests that it is related in part also to the interaction between the parts of the chains close to the wall (for which $\Delta \boldsymbol{P}_x$ is bigger) and those moving slowly in the center of the system, i.e., to the velocity gradient. Most probably the outer parts which move faster extend the chain too much at first because slowly moving parts in the center are ''anchored''. Then the chain relaxes, decreasing the x-coordinate of $\boldsymbol{R}_g$ (c.f. Fig. 11b) which reduces the difference in flow velocity experienced by different parts. This effect is clearly observed both in unipolar and bipolar flows which means that the modification of melt velocity

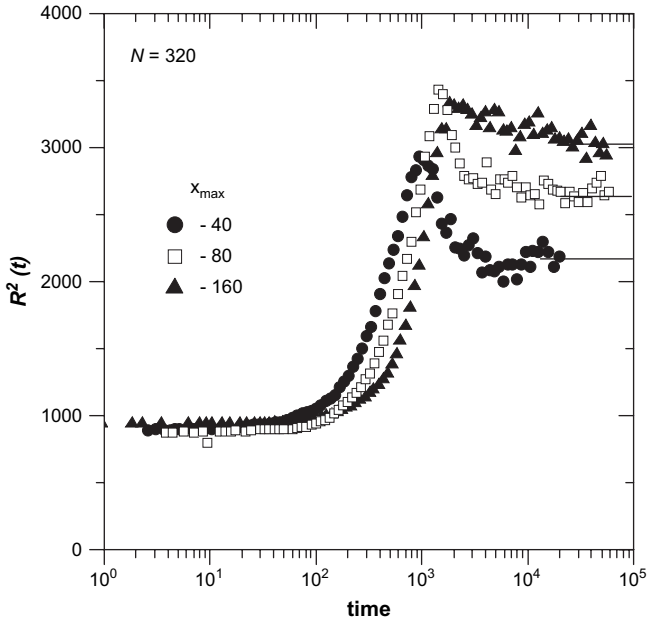

Fig. 17. Time dependence of the mean square end-to-end distance for various x_{max}. Bipolar flow, $\Delta \boldsymbol{P}_{max} = 0.8$. Horizontal lines indicate corresponding equilibrium $\boldsymbol{R}^2$ values.

near the wall is of secondary importance. The overshoot decreases with decreasing N and for $N < 40$ it becomes negligible, even in confined systems with $x_{max} = 20$.

In all simulated cases the chain dynamics is asymmetric due to the presence of non-penetrable walls. Additional asymmetry is induced by the shear stress. Therefore it is interesting to examine the combined effect of the walls and shear on the time dependence of mean-square displacements in x-, y-, and z-directions. These effects were not clearly seen in the previous figures (Figs. 10 and 15) because for the chain length $N = 640$ it would require unacceptably long computation time. Fig. 18 presents x-, y- and z-components of the displacement in the flowing and non-flowing systems for $N = 40$. It can be seen that, as for $N = 640$, the square dependence on time is observed for the z-component, while the x-component tends to level off at around $0.16\, x_{max}^2$ (marked by the horizontal lines) due to the restriction of displacement in this direction by the limiting walls. Please note that for such a short chain, the slope of the y-component (below and above the range in which coil deformation and orientation take place) is equal to 1.0, as predicted by the Rouse model. The x-components also follow $t^{1.0}$ law at short times, when confinement effects are not important yet.

For smaller wall spacing and bipolar bias one can clearly see also another effect of the confined space: at long times the z-component also does not follow the square law but its slope gradually decreases from two to one (the slope indicated in the figure). This effect is due to the diffusion of the chains in the x-direction. A chain initially flowing say in the positive direction must diffuse after some time to the other half of the system where the probability bias is reversed and it begins to flow back. In other words the bipolar flow leads to oscillations of chain displacement and increases its mean value but the asymptotic behavior is the same as for the non-flowing system – it follows normal diffusion law. This is of course not the case for the unipolar flow, where the move probability is biased in the same direction in all the system. Therefore at least some results obtained for these two cases are not exactly equivalent.

It should be noted that according to Pai-Pandiker et al. [22] the effect of confinement on static properties of polymer chains is observed when wall spacing is smaller than $2\boldsymbol{R}_{g_0}$ ($\boldsymbol{R}_g$ of the unconstrained chain), regardless of the molecular weight. In the case shown in Fig. 18 $N = 40$ and $\boldsymbol{R}_{g_0} = 4.2$. Thus even the smallest wall spacing used in this work is well above this limit and the biggest is nearly 20 times bigger than $\boldsymbol{R}_{g_0}$. In our simulations we should be in all cases in the practically unperturbed regime, i.e., even in one of the 'most confined' case $N = 320$ and $x_{max} = 40$ we have $\boldsymbol{R}_{g_0} = 12.2$, hence $\boldsymbol{R}_{g_0} < 2\boldsymbol{x}_{max}$. In the flowing system the chains can be expected to be even less perturbed as we should rather compare x_{max} with $\boldsymbol{R}_{g_x}$ which is smaller than $\boldsymbol{R}_{g_0}$ (e.g. for $N = 320$ and $\Delta\boldsymbol{P}_{max} = 0.8$ $\boldsymbol{R}_{g_x}^2$ decreases almost by one half under shear). Therefore the confinement effects in dynamic properties of the flowing system are clearly seen also for the systems which are relatively big – by *ca.* an order of magnitude bigger as compared with those in which space confinement effects in the static properties of non-flowing melts are observed.

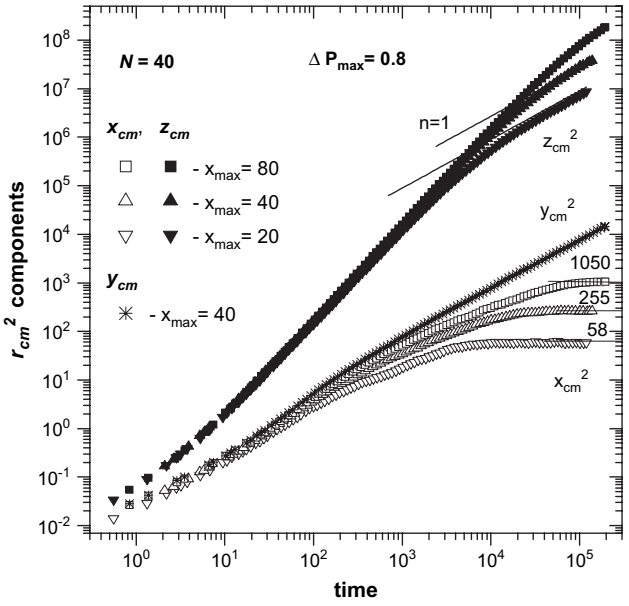

Fig. 18. Wall spacing effect on x-, y- and z-components of the mean square chain center of mass displacements. $N = 40$, $x_{max} = 20$, 40, 80, $\Delta\boldsymbol{P}_{max} = 0.8$. Solid lines in the top-right corner show slopes corresponding to linear time dependence (normal diffusion).

5. Conclusions

The presented results of MC simulations of polymer melts show that the chain dynamics and diffusion under shear stress are significantly different than in the equilibrium melt, in agreement with experiments and previous simulations. The shear influence is strongly dependent on chain length, thus in our simulations for long chains ($N > 10^2$) it is more clearly seen and entanglement effects can be revealed. Relaxation time of long chains decreases by orders of magnitude under shear, following the power law, even for weakly biased systems ($\Delta\boldsymbol{P}_{max} > 0.05$). The time dependence of the end-to-end vector autocorrelation function also changes (being less ''stretched'' under shear). The coil deformation and its orientation in the flow direction increase with increasing chain length. The shear dependence of $\boldsymbol{R}^2$ for various N can be described by a master curve, in qualitative agreement with the results for Rouse chains. Nonlinear dependences on shear stress are observed both in the flow profiles and in the relaxation time shear dependence and such effects are observed for the longest chains studied, even for weakly biased systems.

The simulations of step-shear experiment reveal shear-stress dependent kinetics of chain orientation and coil deformation, which begin, and reach steady-state values, after different times, dependent on shear stresses. Attaining higher equilibrium orientation for big $\Delta\boldsymbol{P}_{max}$ takes place after much shorter time. The chain relaxation shows a different time dependence under shear, characteristic in an acceleration after some time, close to the relaxation time. There is a qualitative difference between chain dynamics in simulated step-shear and melt relaxation experiments. In the latter case relaxation is much slower, practically identical with that of the relaxed melt, not subjected to shear.

The space confinement strongly affects chain dynamics under shear, even when the wall distance is much bigger than $2R_{g_0}$ of the chains under study. Steady-state values of R_g decrease with increasing confinement and they are attained after shorter time.

Diffusion of beads and chains in the flowing melt is also strongly modified by shear stress, including the displacements in the *x*- and *y*-directions (perpendicular to the shear direction). The diffusion of the chain center of mass shows an anomalous behavior (sub- or superdiffusion) in all directions as a result of the space confinement and shear.

In summary we show that in spite of the limitations of MC simulation method used, it is possible to reproduce at least qualitatively most of the shear effects known from the experiment and NMD simulations. Using CMA algorithm we could, however, simulate long, entangled chains on big lattices. It made possible the investigations of microscopic phenomena related to asymmetry of the system dynamics due to flow and space confinement.

Acknowledgement

Financial support of Polish Ministry of Science and Education under project No. 3 T08E 41 26 is acknowledged.

References

[1] Birley AW, Haworth B, Batchelor J. Physics of plastics, processing, properties and materials engineering. Munich: Hanser Publishers; 1992.
[2] Mark JE, Eisenberg A, Graesley WW, Mandelkern L, Samulski ET, Keonig JL, et al. Physical properties of polymers. Washington: ACS; 1993.
[3] Ferry JD. Viscoelastic properties of polymers. New York: Wiley; 1992.
[4] De Gennes PG. Scaling concepts in polymer physics. Ithaca, NY: Cornell University Press; 1979.
[5] Kröger M. Phys Rep 2004;390:453–551.
[6] Gupta SA, Cochran HD, Cummings PT. J Chem Phys 1997;107:10316–26.
[7] Gupta SA, Cochran HD, Cummings PT. J Chem Phys 1997;107:10327–34.
[8] Gupta SA, Cochran HD, Cummings PT. J Chem Phys 1997;107:10335–43.
[9] Katz S, Lebowitz JL, Spoon H. J Stat Phys 1984;34:497–502.
[10] Baschnagel J, Binder K. Macromol Theory Simul 1996;5:417–48.
[11] Pakula T. J Macromol Sci Phys B 1998;37:181–99.
[12] Gleiman S, Dorgan J. J Chem Phys 2000;112:6073–83.
[13] Mavrantzas VG, Theodoru DN. Macromolecules 1998;31:6310–32.
[14] Mavrantzas VG, Theodoru DN. Macromol Theory Simul 2000;9:500–15.
[15] Pakula T. Macromolecules 1987;20:679–82.
[16] Pakula T, Geiler S. Macromolecules 1987;20:2909–14.
[17] Gauger A, Wayersberg A, Pakula T. Macromol Theory Simul 1993;2:531.
[18] Pakula T. Recent Res Dev Polym Sci 1996;1:101–18.
[19] Pakula T, Vlassopoulos D, Fytas G, Roovers J. Macromolecules 1998;31:8931–40.
[20] Pakula T, Jeszka K. Macromolecules 1999;32:6821–30.
[21] Pakula T. J Chem Phys 1991;95:4685–90.
[22] Pai-Pandiker RS, Dorgan JR, Pakula T. Macromolecules 1997;30:6348–52.
[23] Pakula T, Geyler S, Edling T, Boese D. Rheol Acta 1996;35:631–44.
[24] Aoyagi T, Takimoto J, Doi M. J Chem Phys 2001;115:552–9.
[25] Ganazzoli F, Tacconelli A. Macromol Theory Simul 1998;7:79–90.
[26] Doi M, Edwards SF. Theory of polymer dynamics. Oxford: Oxford, Clarendon Press; 1986.
[27] Paul W. Chem Phys 2002;284:59–66.
[28] Baumgartner A, Binder K. J Chem Phys 1981;75:2994.
[29] Kremer K. Macromolecules 1983;16:1632–8.
[30] Yamamoto T, Mori N. JSME Int J B Fluid Therm Eng 2004;47:1–8.
[31] Yamamoto R, Onuki A. Phys Rev E 2004;70:041801.
[32] Xu G, Ding J, Yang Y. Macromol Theory Simul 1998;7:129–40.
[33] Andrews NC, McHugh AJ, Schieber JD. J Rheol 1998;42:281–305.
[34] Menezes EV, Graessley WW. J Polym Sci Polym Phys Ed 1982;20:1817–33.